Complete Mechanical Regularization in Image Correlation

A. MENDOZA[a,b], J. NEGGERS[a], F. HILD[a], S. ROUX[a]

a. LMT (ENS Paris-Saclay/CNRS/Univ. Paris-Saclay), 94235 Cachan, France
b. Safran Tech, 78772 Magny les Hameaux, France

Résumé :

Un schéma de régularisation générique pour la Corrélation d'Images Numérique (CIN) et la Corrélation d'Images Volumiques (CIV) basé sur la méthode de "l'écart à l'équilibre" est présenté. Cette régularisation "complète" fournit un cadre unifié pour le traitement des extremités d'objet (surfaces) ainsi que dans le volume, tout en distinguant les rôles joués par les différentes catégories d'extremités (Neumann ou Dirichlet) dans les tests mécaniques. Un test expérimental valide la robustesse et la précision de la méthode.

Abstract :

A generic regularization scheme for Digital Image Correlation (DIC) and Digital Volume Correlation (DVC) based on the "equilibrium gap" method is presented. This "complete" regularization provides a unified framework for handling the object boundaries (surfaces) as well as the bulk, while also distinguishing the roles that different boundaries (Neumann or Dirichlet) play in mechanical tests. An experimental test validates the robustness and accuracy of the method.

Mots clefs : digital image correlation, digital volume correlation, mechanical regularization, equilibrium gap

1 Introduction

Digital Image Correlation (DIC) and Digital Volume Correlation (DVC) are popular techniques to measure displacement fields from 2D and 3D image pairs, respectively [1]. These image registration techniques face a considerable challenge, namely, their *ill-posedness* [2, 3]. In fact, the limited available information (*i.e.*, brightness levels) leads to an unavoidable compromise between the measurement uncertainty and the spatial resolution [4].

A method for overcoming this limitation is to assume the displacement field to be *continuous* over the entire region of interest (ROI). Hence, it can be decomposed over basis functions that fulfill this constraint, such as those used in the Finite Element (FE) method. The imposed inter-dependence (coupling) between all degrees of freedom leads to the so-called *global* DIC and DVC methods [5, 6]. They differ from their *local* counterparts [1, 7] that do not assume any continuity in the sought displacement fields.

Additionally, regularization techniques [8] can be employed to further circumvent the ill-posedness of the registration [2]. In particular, in the context of experimental mechanics, it is natural to seek a displacement field that best registers the images while also being mechanically admissible. Such is the goal of the so-called "mechanical regularization" based on the *equilibrium gap* method [9, 10]. This regularization constrains the displacement field to one that locally follows a linear elastic behavior. It is noteworthy that such elastic regularization has proven useful even when the actual behavior is more complex [10].

Unfortunately, this approach by itself is not capable of applying the adequate regularization to each type of boundary surface present in the analysis. In fact, the guiding principle is only valid for the bulk and free-surfaces of the studied sample. For such reason, in Ref. [11], the authors proposed an approach that mimics the bulk, as if those surfaces had an elasticity of their own in addition to the bulk (as a kind of "surface tension"). However, the link between both models (bulk and surfaces) is relatively poor.

In the present paper, an extension to mechanical regularization is presented. It distinguishes the roles that different boundaries (Neumann or Dirichlet) play and treats them accordingly. Moreover, it does not require further (nor customized) developments other than those already postulated by the *equilibrium gap*. It thus provides a single framework for handling the object boundaries both in 2D as in 3D without any modification.

2 Method

2.1 Image Correlation

The registration of the images in the reference configuration $f(\boldsymbol{x})$ and deformed configuration $g(\boldsymbol{x})$ is based on the brightness conservation assumption

$$f(\boldsymbol{x}) = g(\boldsymbol{x} + \boldsymbol{u}(\boldsymbol{x})) \tag{1}$$

where $\boldsymbol{u}(\boldsymbol{x})$ is the sought displacement field that minimizes the L_2 norm of the so-called "correlation residuals" over the entire ROI Ω

$$\Phi_c = \sum_{\Omega} \left(g(\boldsymbol{x} + \boldsymbol{u}(\boldsymbol{x})) - f(\boldsymbol{x})\right)^2 \tag{2}$$

Given that the minimization of Φ_c is an *ill-posed* problem, the displacement field $\boldsymbol{u}$ is decomposed over a set of chosen kinematic fields $\boldsymbol{\psi}_i$, such as those used in the FE method

$$\boldsymbol{u}(\boldsymbol{x}) = \sum_i u_i \boldsymbol{\psi}_i(\boldsymbol{x}) \tag{3}$$

Then, the registration problem consists in minimizing Φ_c with respect to all the unknown amplitudes u_i. A Newton-Raphson scheme leads to linear systems

$$[\boldsymbol{M}_c]\,\{\delta \boldsymbol{u}\} = \{\boldsymbol{b}\} \tag{4}$$

where the matrix $[\boldsymbol{M}_c]$ is built from the image gradients $\boldsymbol{\nabla} f$ and the shape functions $\boldsymbol{\psi}_i$, the vector $\{\boldsymbol{b}\}$ accounts for the image residuals $\eta(\boldsymbol{x}) = g(\boldsymbol{x} + \tilde{\boldsymbol{u}}(\boldsymbol{x})) - f(\boldsymbol{x})$, with $\tilde{\boldsymbol{u}}$ the current estimate of the

dispalacement field, and $\{\delta \boldsymbol{u}\}$ updates the degrees of freedom u_i gathered in the column vector $\{\boldsymbol{u}\}$ during the iterations.

2.2 Mechanical Regularization

In the spirit of what was introduced earlier, an ideal regularization would be based on the actual mechanical behavior of the studied specimen. Yet, in order to provide a general approach that does not need to be tailored to each individual case, a "simplification" of the aforementioned behavior is in order. It consists in recognizing that locally, unless a localization instability occurs, the sought displacement may often be well described by an elastic problem. This is the spirit of the proposed regularization based on the *equilibrium gap*, namely, the "distance" between the current solution and that which locally satisfies the equilibrium equation for linear elasticity [9, 12, 11, 10]. Such equation satisfies

$$\boldsymbol{\nabla} \cdot \boldsymbol{\sigma} + \boldsymbol{f} = \boldsymbol{0} \tag{5}$$

with the distribution of body forces $\boldsymbol{f}$, and the Cauchy stress tensor $\boldsymbol{\sigma}$. The latter is linearly related to the infinitesimal strain tensor $\boldsymbol{\epsilon}$ with Hooke's tensor $\boldsymbol{C}$. In the context of the FE method, this equation assumes the discretized form

$$[\boldsymbol{K}]\,\{\boldsymbol{u}\} = \{\boldsymbol{f}\} \tag{6}$$

where $[\boldsymbol{K}]$ is the stiffness matrix, $\{\boldsymbol{f}\}$ the vector of nodal forces, and $\{\boldsymbol{u}\}$ collects the nodal displacements associated with the displacement field $\boldsymbol{u}$.

At this point, it is useful to recall the concept of "Neumann" and "Dirichlet" degrees of freedom (DOFs). These terms are usually employed to denote the DOFs for which externally applied tractions or displacements are known, and where conversely displacements or tractions are to be computed, respectively. Then, under this FE discretization, the studied DOFs are classified into different groups, namely, those belonging to either Neumann $\mathcal{S}_{\mathcal{N}}$ or Dirichlet $\mathcal{S}_{\mathcal{D}}$ boundaries, and the remaining (bulk) $\mathcal{B}$ ones.

Hence, given the identity matrix $\boldsymbol{I}$ that accounts for all the DOFs in the mesh, the corresponding projection matrices $\boldsymbol{D}$ (valued 1 for the DOFs that pertain to the corresponding group and valued 0 otherwise) are related by

$$\boldsymbol{I} = \boldsymbol{D}_{\mathcal{B}} + \boldsymbol{D}_{\mathcal{S}_{\mathcal{N}}} + \boldsymbol{D}_{\mathcal{S}_{\mathcal{D}}} \tag{7}$$

In particular, the Dirichlet boundary DOFs are listed with respect to each (Dirichlet) surface $\mathcal{S}_i$

$$\boldsymbol{D}_{\mathcal{S}_{\mathcal{D}}} = \textstyle\sum_i \boldsymbol{D}_{\mathcal{S}_i} \tag{8}$$

Then, *mechanical regularization* consists in minimizing the L_2 norm of the unbalanced nodal forces for all bulk and Neumann DOFs

$$\Phi_m(\{\boldsymbol{u}\}) = \left\| [\boldsymbol{K}_m]\,\{\boldsymbol{u}\} - \{\boldsymbol{f}\} \right\|^2 \tag{9}$$

where Φ_m corresponds to the equilibrium gap for the bulk and Neumann surfaces DOFs, as given by the partial stiffness matrix

$$[\boldsymbol{K}_m] = \left([\boldsymbol{D}_{\mathcal{B}}] + \left[\boldsymbol{D}_{\mathcal{S}_{\mathcal{N}}}\right] \right) [\boldsymbol{K}] \tag{10}$$

However, the same argument cannot be made for the remaining DOFs (*i.e.*, those belonging to the Dirichlet surfaces) because the external forces are unknown. Since the nodal forces for these DOFs do not vanish, it is proposed to introduce a new penalization term that tends toward a common local orientation

and similar magnitude. Hence, a penalty is introduced on the quadratic norm of the gradient along each surface $\mathcal{S}_i$ of each component of the normal traction. Rapid variations of the unbalanced forces along the Dirichlet surfaces are thus dampened out (this is not the case for long wavelength components).

This surface regularization cost function is written as

$$\Phi_{\mathcal{S}_i} = \|\boldsymbol{\nabla}\left(\boldsymbol{\sigma}\cdot\boldsymbol{n}\right)\|^2 \quad \text{for } \boldsymbol{x}\in\mathcal{S}_i \tag{11}$$

where $\boldsymbol{n}$ is the outward surface normal. In the context of the FE method, for each surface $\mathcal{S}_i$, this equation assumes the discretized form

$$\Phi_{\mathcal{S}_i}(\{\boldsymbol{u}\}) = \{\boldsymbol{u}\}^\intercal[\boldsymbol{K}_{\mathcal{S}_i}]^\intercal\left[\boldsymbol{L}\right]\left[\boldsymbol{K}_{\mathcal{S}_i}\right]\{\boldsymbol{u}\} \tag{12}$$

where $\Phi_{\mathcal{S}_i}$ corresponds to the penalization for DOFs belonging to the (Dirichlet) surface $\mathcal{S}_i$, as given by the partial stiffness matrix

$$\left[\boldsymbol{K}_{\mathcal{S}_i}\right] = \left[\boldsymbol{D}_{\mathcal{S}_i}\right]\left[\boldsymbol{K}\right] \tag{13}$$

and $[\boldsymbol{L}]$ corresponds to the discrete Laplace-Beltrami operator [13] (*i.e.*, the FE discretization of the L_2 norm of the surface gradient operator).

Finally, the *complete* mechanical regularization is obtained by minimizing the weighted sum of the previously defined functionals

$$\Phi_t(\{\boldsymbol{u}\}) = \alpha_c\Phi_c(\{\boldsymbol{u}\}) + \alpha_m\Phi_m(\{\boldsymbol{u}\}) + \sum_i \alpha_{\mathcal{S}_i}\Phi_{\mathcal{S}_i}(\{\boldsymbol{u}\}) \tag{14}$$

with the prefactors

$$\alpha_o = \frac{\omega_o}{\sum_j \omega_j}\cdot\frac{1}{E_o} \tag{15}$$

composed of a normalizing term E_0 that accounts for the "energy" related to each functional (as measured by their response to a pure shear trial field), and of a weighting term ω proportional to characteristic (regularization) lengths ξ defined for each type of DOF.

The minimization of Φ_t is still performed via a Newton-Raphson scheme, which leads to new linear systems

$$\left([\boldsymbol{M}_c] + \left[\boldsymbol{M}_{\text{reg}}\right]\right)\{\delta\boldsymbol{u}\} = \{\boldsymbol{b}\} - \left[\boldsymbol{M}_{\text{reg}}\right]\{\boldsymbol{u}\} \tag{16}$$

with the regularization matrix

$$\left[\boldsymbol{M}_{\text{reg}}\right] = E_c\left(\frac{\omega_m}{E_m}\left[\boldsymbol{K}_m\right]^\intercal\left[\boldsymbol{K}_m\right] + \frac{\omega_{\mathcal{S}_i}}{E_{\mathcal{S}_i}}\left[\boldsymbol{K}_{\mathcal{S}_i}\right]^\intercal\left[\boldsymbol{L}\right]\left[\boldsymbol{K}_{\mathcal{S}_i}\right]\right) \tag{17}$$

3 Results

The goal of this section is to present the advantages of the technique for a tensile test performed on a pre-cracked sample made of spheroidal graphite cast iron. The sample comes from a bigger specimen that was pre-fatigued with a load shedding technique in order to avoid having a large plastic zone around the crack front [14].

Seven tomographic scans were acquired at increasing loading stages using a micro-CT scanner (North Star Imaging X50+) with a resolution of 7 μm and a chosen ROI of $4.2\times1.9\times1.6$ mm. Scans **`S0`**,

S1 and **S2** are obtained in the elastic regime of the sample, thus the crack does not open very much. Conversely, crack opening is more pronounced in scans **S3** and **S4** when the sample has yielded. Last, ductile tearing occurs for scans **S5** and **S6**. A mid-thickness slice of each scan is shown in figure 1 alongside the load level at which each scan was acquired.

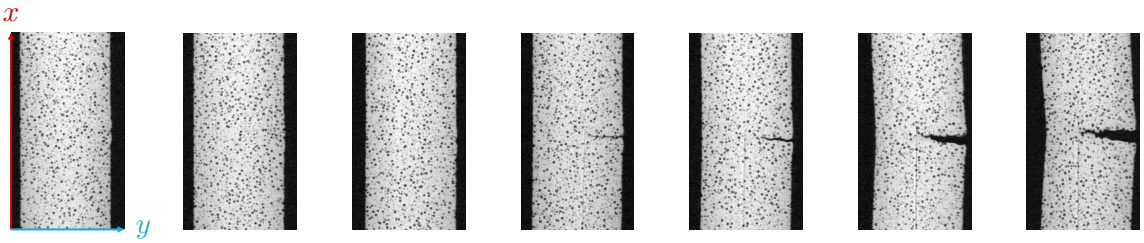

(a) **S0**, 61 N (b) **S1**, 196 N (c) **S2**, 282 N (d) **S3**, 646 N (e) **S4**, 720 N (f) **S5**, 805 N (g) **S6**, 730 N

Figure 1: (x-y) mid-thickness sections for all scans showing the test history (crack opening and tearing) with the respective loads

The first scan **S0** is chosen as the reference for the correlation procedure. It drives an automatic meshing procedure that provides an unstructured FE mesh fitted to the actual geometry of the sample. The mesh is constructed using tetrahedral elements of characteristic length $\ell = 25$ vx. While such length could be considered small (as compared to the material microstructure), it was chosen on purpose so that unregularized DVC would encounter difficulties for converging. Furthermore, since the lateral surfaces are traction-free, they are considered of Neumann type. However, the upper and bottom surfaces cut through the sample. Therefore they are considered of Dirichlet type. A volume representation of scan **S0** as well as the obtained mesh and the Dirichlet surfaces are shown in figure 2.

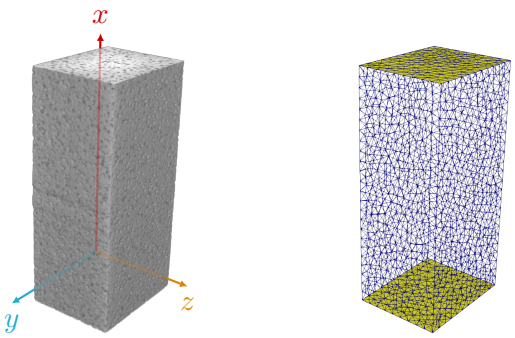

(a) (b)

Figure 2: (a) Volume rendering of the reference scan **S0** and (b) corresponding FE mesh with the Dirichlet surfaces highlighted

Three cases are studied: (i) **none**: with no regularization, (ii) **bulk**: using only bulk regularization, and (iii) **all**: using bulk and surface regularization. All three cases are based on global DVC, and two are complemented by the corresponding regularization. Hence, the so-called "**none**" case, which corresponds to the standard version of global DVC [15], can be considered as a "regularized" version of the more common (*i.e.*, local) DVC approaches [7, 16] since displacement continuity is enforced over the whole ROI. Thus, when convergence reveals difficult without regularization, most of the existing local DVC codes would encounter even more obstacles for converging under similar circumstances.

The correlation procedure is carried out in an iterative manner (*i.e.*, the solution found for the previous scan is used as initialization for the current one) under a multi-scale scheme that progressively relaxes

the regularization (via the regularization lengths). The final regularization lengths are set to $\xi_m = 2\ell$ and $\xi_{\mathcal{S}_i} = 2\xi_m$. Also, each correlation procedure is limited to a chosen maximum of $N_{it} = 200$ iterations.

Next, it is proposed to analyze the results from the perspective of the global correlation residual

$$\sigma = \frac{1}{\Delta f}\sqrt{\frac{1}{\mathcal{N}_\Omega}\sum_{\Omega}\left(g(\boldsymbol{x}+\boldsymbol{u}(\boldsymbol{x})) - f(\boldsymbol{x})\right)^2} \tag{18}$$

normalized by the dynamic range $\Delta f = \max(f) - \min(f)$.

These residuals σ are computed for each of the deformed configurations. They are reported in table 1 along with the number of iterations N_{it} each analysis took. With regard to the baseline measurement (between **`S0`** and **`S1`**), the **`none`** code does not converge (by design). Conversely, **`bulk`** and **`all`** regularizations lead to convergence with $\sigma = 3.24\%$, a low value when dealing with tomographic data. For the remaining scans, it should be noted that all computations converged for the **`all`** case. Yet only two and zero calculations converged for the **`bulk`** and **`none`** regularizations, respectively. Even in the **`bulk`** cases that converged (*i.e.*, **`S2`**, **`S4`**), it required a significantly higher number of iterations than in the **`all`** case. This observation shows the gain associated with surface regularization.

Table 1: Number of iterations and final residual for different regularization strategies (converged results are shown in **boldface**). All strategies are based on global DVC [15]

	`none`		**`bulk`**		**`all`**	
	N_{it}	σ	N_{it}	σ	N_{it}	σ
`S1`	200	5.02%	**94**	**3.24%**	**13**	**3.24%**
`S2`	200	10.15%	**176**	**3.26%**	**18**	**3.25%**
`S3`	200	11.23%	200	5.09%	**16**	**4.44%**
`S4`	200	11.38%	**196**	**3.54%**	**14**	**3.49%**
`S5`	200	11.29%	200	4.13%	**33**	**4.11%**
`S6`	200	11.03%	200	5.68%	**65**	**5.37%**

As it can be seen from figure 3, the top-most surface is challenging the **`bulk`** case. The correlation with no surface regularization (*i.e.*, **`none`** and **`bulk`**) cannot handle such phenomenon. However, just by taking this surface into consideration (**`all`**), the problem is easily solved. These results illustrate the beneficial effect of the proposed surface regularization.

4 Conclusion

The complete mechanical regularization proposed herein opens many possibilities in the field of Digital Image and Volume Correlation. First, since the technique is an extension to the bulk mechanical regularization, it naturally inherits all its benefits such as providing lower levels of uncertainty, even when dealing with images of poor quality.

The reported results highlight the benefits of complete mechanical regularization. It provides fast convergence, which, in practical terms, allows even complex cases to be treated both robustly and fast. This behavior is desirable even in simple cases that may not "require" regularization, since they can be swiftly solved using lesser iterations.

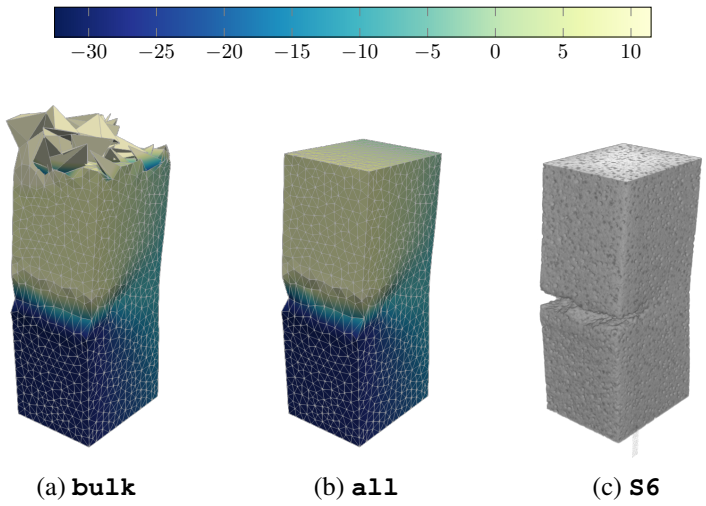

(a) **bulk** (b) **all** (c) **S6**

Figure 3: (a)-(b) Longitudinal displacement (expressed in voxels) for two regularization procedures and (c) volume rendering of the deformed scan **S6**

Additionally, given that the proposed formulation builds upon concepts from the Finite Element method, it is applicable to any type of element (triangles, tetrahedra) or mesh (structured or not) in either two-dimensions or three-dimensions. As such, objects with arbitrarily *complex* boundaries can be studied in their entirety using DIC or DVC, accordingly. Furthermore, each of these boundaries can be accounted for differently according to the initial conditions.

Last, while the discussion was based on plain linear elasticity, if a better appreciation of the sample constitutive law is available, the corresponding regularization is easily generalized.

Acknowledgments

The authors are very grateful to Prof. J.-Y. Buffière and Dr. N. Limodin for kindly providing and preparing the test sample. They also wish to thank Dr. A. Bouterf and Mr. B. Smaniotto for performing the test reported herein. This work was supported by the PRC MECACOMP, project co-funded by DGAC and Safran group, involving Safran group companies, ONERA, CNRS and other academic partners. This work has also benefited from the support of the French "Agence Nationale de la Recherche" through the "Investissements d'avenir" program under the reference "ANR-10-EQPX-37 MATMECA".

References

[1] H. Schreier, J.-J. Orteu, and M. A. Sutton. *Image Correlation for Shape, Motion and Deformation Measurements*. Springer US, 2009. ISBN: 978-0-387-78746-6. DOI: 10.1007/978-0-387-78747-3.

[2] M. Bertero, T. A. Poggio, and V. Torre. "Ill-Posed Problems in Early Vision". In: *Proceedings of the IEEE* 76.8 (1988), pp. 869–889. ISSN: 15582256. DOI: 10.1109/5.5962.

[3] F. Hild and S. Roux. "Digital Image Correlation". In: *Optical Methods for Solid Mechanics. A Full-Field Approach*. Ed. by P. Rastogi and E. Hack. Weinheim (Germany): Wiley-VCH, 2012. Chap. 5, pp. 183–228.

[4] M. Bornert et al. “Assessment of digital image correlation measurement errors: Methodology and results”. In: *Experimental Mechanics* 49.3 (2009), pp. 353–370. ISSN: 00144851. DOI: 10.1007/s11340-008-9204-7.

[5] G. Besnard, F. Hild, and S. Roux. “Finite-element displacement fields analysis from digital images: Application to Portevin-Le Châtelier bands”. In: *Experimental Mechanics* 46.6 (2006), pp. 789–803. ISSN: 00144851. DOI: 10.1007/s11340-006-9824-8.

[6] S. Roux et al. “Three-dimensional image correlation from X-ray computed tomography of solid foam”. In: *Composites Part A: Applied Science and Manufacturing* 39.8 (2008), pp. 1253–1265. ISSN: 1359835X. DOI: 10.1016/j.compositesa.2007.11.011.

[7] B. K. Bay et al. “Digital volume correlation: Three-dimensional strain mapping using X-ray tomography”. In: *Experimental Mechanics* 39.3 (1999), pp. 217–226. ISSN: 0014-4851. DOI: 10.1007/BF02323555.

[8] A. N. Tikhonov and V. Y. Arsenin. *Solutions of ill-posed problems*. Winston, 1977.

[9] J. Réthoré, S. Roux, and F. Hild. “An extended and integrated digital image correlation technique applied to the analysis of fractured samples”. In: *European Journal of Computational Mechanics* 18.3-4 (2009), pp. 285–306. ISSN: 17797179. DOI: 10.3166/ejcm.18.285-306.

[10] T. Taillandier-Thomas et al. “Localized strain field measurement on laminography data with mechanical regularization”. In: *Nuclear Instruments and Methods in Physics Research, Section B: Beam Interactions with Materials and Atoms* 324 (Apr. 2014), pp. 70–79. ISSN: 0168583X. DOI: 10.1016/j.nimb.2013.09.033.

[11] Z. Tomicevic, F. Hild, and S. Roux. “Mechanics-Aided Digital Image Correlation”. In: *The Journal of Strain Analysis for Engineering Design* 48.5 (2013), pp. 330–343.

[12] H. Leclerc et al. “Voxel-Scale Digital Volume Correlation”. In: *Experimental Mechanics* 51.4 (2011), pp. 479–490. ISSN: 00144851. DOI: 10.1007/s11340-010-9407-6.

[13] M. Reuter et al. “Discrete Laplace-Beltrami operators for shape analysis and segmentation”. In: *Computers and Graphics (Pergamon)* 33.3 (June 2009), pp. 381–390. ISSN: 00978493. DOI: 10.1016/j.cag.2009.03.005.

[14] N. Limodin et al. “Crack closure and stress intensity factor measurements in nodular graphite cast iron using three-dimensional correlation of laboratory X-ray microtomography images”. In: *Acta Materialia* 57.14 (Aug. 2009), pp. 4090–4101. ISSN: 13596454. DOI: 10.1016/j.actamat.2009.05.005.

[15] S. Roux and F. Hild. “Digital image mechanical identification (DIMI)”. In: *Experimental Mechanics* 48.4 (2008), pp. 495–508.

[16] B. K. Bay. “Methods and applications of digital volume correlation”. In: *The Journal of Strain Analysis for Engineering Design* 43.8 (2008), pp. 745–760. ISSN: 0309-3247. DOI: 10.1243/03093247JSA436.